

# **Interfacial Dipole Engineering via Boronic Acid-Based Self-Assembled Monolayers in Inverted Tin-Lead Perovskite Solar Cells with ideal band gap**

*Safalmani Pradhan<sup>1,\*</sup>, Huān Bi<sup>1</sup>, Gaurav Kapil<sup>1</sup>, Aruto Akatsuka<sup>3</sup>, Ajay Kumar Baranwal<sup>4</sup>, Dandan Wang<sup>2</sup>, Dong Liu<sup>2</sup>, Suraya Shaban<sup>1</sup>, Takeshi Kitamura<sup>1</sup>, Shahrir Razey Sahamir<sup>1</sup>, Yasuhiro Fujiwara<sup>1</sup>, Jiaqi Liu<sup>1,\*</sup>, Hiroshi Segawa<sup>5</sup>, Hiroyuki Yoshida<sup>3</sup>, Qing Shen<sup>1,2,\*</sup>, Shuzi Hayase<sup>1,\*</sup>*

<sup>1</sup>Info-Powered Energy System Research Center, The University of Electro-Communications, 1-5-1 Chofugaoka, Chofu, Tokyo, 182-8585, Japan

<sup>2</sup>Graduate School of Informatics and Engineering, The University of Electro-Communications, 1-5-1 Chofugaoka, Chofu, Tokyo 182-8585, Japan

<sup>3</sup>Graduate School of Engineering, Chiba University, 1-33 Yayoi-cho, Inage-ku, 263-8522, Chiba, Japan

<sup>4</sup>Department of Electronics and Communications Engineering, Madan Mohan Malaviya University of Technology, Gorakhpur, Uttar Pradesh, 273010, India

<sup>5</sup>Department of General Systems Studies, Graduate School of Arts and Sciences, The University of Tokyo, 3-8-1, Komaba, Meguro-ku, Tokyo 153-8902, Japan

**Corresponding Authors:** [safalmani@uec.ac.jp](mailto:safalmani@uec.ac.jp); [liujiaqi@uec.ac.jp](mailto:liujiaqi@uec.ac.jp); [shen@pc.uec.ac.jp](mailto:shen@pc.uec.ac.jp); [hayase@uec.ac.jp](mailto:hayase@uec.ac.jp)

## 1. Materials and Methods

### (i) Chemicals and solvents:

All chemicals and solvents used for preparing the perovskite precursor solution were used as received, without any further purification. Formamidinium Iodide (FAI,  $\text{NH}_2\text{CH}=\text{NH}_2\text{I}$ ), Formamidinium Bromide (FABr,  $\text{NH}_2\text{CH}=\text{NH}_2\text{Br}$ ) and Phenylethylammonium chloride (PEACl) were purchased from TCI, Japan. Lead (II) Iodide ( $\text{PbI}_2$ , 99.999% trace metals basis, perovskite grade), Tin (II) Iodide ( $\text{SnI}_2$ , 99.99% trace metals basis), Tin (II) Fluoride ( $\text{SnF}_2$ ), and Rubidium Iodide (RbI, 99.9% trace metals basis) were purchased from Sigma-Aldrich, Japan. Cesium Bromide (CsBr) was acquired from Alfa Aesar, Japan. The electron transport layers (ETLs) that were used during the fabrication of perovskite solar cells (PSCs) such as, [6,6]-phenyl- $\text{C}_{61}$ -butyric acid methyl ester (PCBM) and fullerene ( $\text{C}_{60}$ ) were purchased from Sigma-Aldrich, Japan. Among the Hole Transport Layers (HTLs) that were used for the fabrication of PSCs, 4-nitrophenyl boronic acid was purchased from Sigma-Aldrich, Japan. Other HTLs namely, 4-cyanophenyl boronic acid (4-CPBA), 4-trifluoromethylphenyl boronic acid (4-TFPBA), and 4-fluorophenyl boronic acid (4-FPBA), [2-(3,6-Dimethoxy-9H-carbazol-9-yl)ethyl]phosphonic Acid (MeO-2PACz) were purchased from TCI, Japan. Additional chemicals used in the experiments including the passivating agent ethylenediamine (EDA, ReagentPlus®,  $\geq 99\%$ ), bathocuproine (BCP, sublimed grade, 99.99% trace metals basis), were purchased from Sigma-Aldrich, Japan. Anhydrous N,N-dimethylformamide (DMF, 99.8%), anhydrous dimethyl sulfoxide (DMSO,  $\geq 99.9\%$ ), anhydrous toluene (99.8%), anhydrous chlorobenzene (CB, 99.8%), and anhydrous isopropyl alcohol (IPA, 99.5%), used during the experiment were purchased from Sigma-Aldrich, Japan.

## **(ii) Preparation of Perovskite precursor solution**

( $\text{Cs}_{0.15}\text{FA}_{0.8}\text{Rb}_{0.05}\text{Sn}_{0.25}\text{Pb}_{0.75}\text{I}_{2.5}\text{Br}_{0.5}$ ):

The perovskite precursor solution ( $\text{Cs}_{0.15}\text{FA}_{0.8}\text{Rb}_{0.05}\text{Sn}_{0.25}\text{Pb}_{0.75}\text{I}_{2.5}\text{Br}_{0.5}$ ) (1.5 M) was prepared by mixing 47.88 mg (0.15 mol) CsBr, 116.08 mg (0.45 mol) FAI, 65.61 mg (0.35 mol) FABr, 15.93 mg (0.05 mol) RbI, 139.70 mg (0.25 mol)  $\text{SnI}_2$ , 518.64 mg (0.75 mol)  $\text{PbI}_2$ , 5.88 mg (0.025 mol)  $\text{SnF}_2$ , and 4 mg, (2.1 mol%) PEACl in 1 ml of DMF:DMSO (4:1, v/v) solution. The precursor solution was then kept under stirring for 3 hours at room temperature inside the glove box.

## **(iii) Fabrication of Perovskite Solar cell (PSC):**

The perovskite solar cell (PSC) was fabricated on fluorine-doped tin oxide (FTO) coated glass substrates ( $17 \Omega \text{ sq}^{-1}$ , Astellatech, Japan) with dimensions of  $2 \text{ cm} \times 2 \text{ cm}$ . The FTO substrates were sequentially cleaned in an ultrasonic bath for 15 minutes each with: (i) a lab detergent solution (SCAT 20-X, Japan) in distilled water, (ii) distilled water, (iii) acetone (Wako, Japan), and (iv) isopropyl alcohol (IPA) (Wako, Japan). After drying, the substrates were subjected to plasma treatment (Electronic Diener, Plasma Surface Technology, Germany) for 5 minutes. Subsequently, 1 mg/mL solution (stirred overnight) of different hole transport layers (HTLs), i.e., Self-Assembled Monolayers (SAMs) in IPA were deposited on the plasma treated FTO substrates. 100  $\mu\text{L}$  solution of SAMs were dropped onto FTO, allowed to rest for  $\sim 5 \text{ s}$ , and then spin-coated at 3000 rpm for 30 s, followed by annealing at  $100 \text{ }^\circ\text{C}$  for 10 min. The films were rinsed with IPA and annealed again at  $100 \text{ }^\circ\text{C}$  for 5 min in order to remove the unbonded SAMs from the surface of FTO. The substrates were then transferred into a nitrogen-filled glovebox for performing further fabrication procedure. The perovskite films were deposited by spin coating 100

$\mu\text{L}$  of perovskite precursor solution onto the SAM-modified FTO substrates using a two-step program: 1000 rpm for 10 s and 4000 rpm for 40 s. At the 30<sup>th</sup> second from the beginning 400  $\mu\text{L}$  of Chlorobenzene (CB) was dropped. This was followed by annealing at perovskite deposited substrates at 100 °C for 10 mins. Following this, the perovskite film was passivated by spin-coating a 0.1 mM solution of ethylenediamine (EDA) in CB at 5000 rpm for 40 s. The passivated perovskite films were then annealed at 70 °C for 10 mins. Subsequently, PCBM (5 mg/mL in chlorobenzene) was spin-coated at 5000 rpm for 40 s and annealed at 70 °C for 10 mins. Finally, C<sub>60</sub> (20 nm), BCP (7 nm), and Ag (150 nm) were sequentially deposited by thermal evaporation under high vacuum ( $\sim 10^{-4}$  to  $10^{-5}$  Pa).

**(iv) Photovoltaic measurement:**

The current-voltage (I-V) characteristics of the PSCs were measured in both forward and reverse scan directions at a scan rate of 10 mV s<sup>-1</sup> using a solar simulator (JIS C 8942 Class MA). The illumination intensity (100 mW cm<sup>-2</sup>) and spectral output of the solar simulator were calibrated using a spectroradiometer (LS-100, Eiko Seiki, Japan). To further confirm the incident power, the light source was calibrated using an amorphous silicon photodetector (BS-520 S/N 007, Bunko Keiki, Japan) in the 300 – 800 nm range and an infrared photodetector (BS-500IR76, Bunko Keiki, Japan) in the 800 – 1200 nm range by measuring the corresponding output currents. To validate the photocurrent obtained from I-V measurements, the external quantum efficiency (EQE) was measured for the samples under a constant photon flux of  $0.5 \times 10^{16}$  photons cm<sup>-2</sup> at each wavelength from 300 to 1000 nm, under direct current mode and without any biasing. All

measurements were carried out under ambient air conditions without device encapsulation, using an optical mask to define the active illumination area of 0.10 cm<sup>2</sup>.

**(v) Ultraviolet-visible (UV-vis) spectra of the perovskite thin-films:**

The absorption spectra were recorded using a UV-Vis-NIR spectrophotometer (V-570, JASCO, Japan) equipped with an integrated sphere setup, capable of measuring absorbance in the wavelength range of 190-2500 nm with a spectral accuracy of  $\pm 1.5$  nm.

**(vi) Determination of Work Function and Valence Band Maximum (VBM):**

The work function and valence band maximum of the samples were measured by ultraviolet photoelectron spectroscopy in Chiba University. He I $\alpha$  radiation from a helium discharge lamp (SPECS, UVS 10/35) was used as the ultraviolet photons source. The He I $\alpha$  photons were incident at an angle of 45° with respect to the sample surface, and the emitted photoelectrons were detected along the surface normal. Measurements were conducted under ultra-high vacuum at a pressure of  $1.4 \times 10^{-6}$  Pa. The kinetic energy of the photoelectrons was analyzed using a hemispherical electron energy analyzer (SPECS, PHOIBOS 100). Vacuum levels were determined from secondary electron cut-off measured by applying a -5 V bias voltage to the sample. The valence band spectra were measured without the bias voltage. Additionally, the energy of the valence band maximum (VBM) was determined using a photoelectron yield spectroscopy (PYS) system (BUNKOKEIKI, KV-205 HK) under high vacuum conditions ( $\sim 10^{-4}$  Pa). The system utilizes a deuterium lamp as a monochromatic light source, which irradiates the sample surface and induces photoemission of electrons. The resulting photocurrent is detected using a sub-picoammeter to accurately determine the onset of photoemission corresponding to the VBM.

**(vii) Surface Morphology investigation:**

A field emission scanning electron microscope (FE-SEM, JEOL JSM-6340) and Schottky field emission scanning electron microscope (SU5000, HITACHI) were employed to analyse the surface morphology of the perovskite thin films. Atomic Force Microscopy (AFM, JEOL-JSPM 5200) was employed to analyse the surface roughness of the perovskite films.

**(viii) X-ray Diffraction (XRD):**

X-ray diffraction (XRD) patterns of the perovskite thin films were obtained using an XRD system (RINT-ULTIMA III, RIGAKU, Japan) equipped with a Cu K $\alpha$  radiation source ( $\lambda = 1.54 \text{ \AA}$ ). The corresponding XRD spectra were fitted using SmartLab Studio II software in order to extract data related to Full-Width at Half Maximum (FWHM), d-spacing, crystal size, etc. of the XRD peaks.

**(ix) X-ray Photoelectron Spectroscopy (XPS):**

X-ray photoelectron spectroscopy (XPS) measurements were performed using a JPS-9200 spectrometer, JEOL to analyze the surface chemical composition. A magnesium (Mg) K $\alpha$  X-ray source ( $h\nu = 1253.6 \text{ eV}$ ) was employed for excitation. The spectra were acquired with a pass energy of 10 eV with a step of 0.1 eV. The measurements were conducted under ultra-high vacuum conditions ( $\sim 10^{-7} \text{ Pa}$ ). Additionally, the relative molecular absorption density of SAM was estimated by X-ray photoelectron spectroscopy in Chiba University. We used the same apparatus for UPS, replacing the UV source with the X-ray source. We used Al K $\alpha$  radiation (1486.6 eV) from the X-ray source (PREVAC,

RS 40B1). The X-rays were incident at an angle of  $25^\circ$ , and the photoelectrons were detected at an angle of  $30^\circ$  with respect to the sample surface. The X-ray source was operated at 60 W, and the pass energy of the electron energy analyzer was set to 60 eV.

**(x) Film thickness:**

The thickness of the perovskite films was measured using coherence scanning interferometry (CSI) (HITACHI, VS1330) with filtered light by using a 530 nm bandpass filter. The scanning was performed over an area of  $1115 \times 1115 \mu\text{m}^2$ .

**(xi) Surface Potential Measurements:**

The kelvin probe force microscope (KPFM, JSPM-5200, JEOL) was utilized for surface potential measurements. The AIOE cantilever (A: 15 kHz, 0.2 N/m, JEOL) was used, where the silicon surface is coated with 5 nm of chromium, and the top surface is coated with 25 nm of platinum.

**(xii) Transient Absorption Spectroscopy (TAS):**

Transient absorption (TA) measurements were conducted using a femtosecond (fs) TA setup, utilizing a titanium/sapphire laser (CPA-2010, Clark-MXR Inc.) with a wavelength of 775 nm, a repetition rate of 1 kHz, and a pulse width of 150 fs for studying the charge carrier dynamics in perovskite thin films. The laser light was split; one part hit a sapphire plate to produce white light for the probe beam, while the other part pumped an optical parametric amplifier (OPA) (a TOAPS from Quantronix) to generate tunable light pulses ranging from 290 nm to 3  $\mu\text{m}$ , used as pump light for sample excitation. Specifically, pump light with a wavelength of 470 nm was employed to excite the perovskite film. Time-resolved TA spectra were captured with a temporal resolution of 100 fs. The probe

delay was varied to record transient spectra at different time intervals after excitation. Kinetic traces were extracted at specific 850 – 870 nm region corresponding to the ground-state bleach (GSB) of the perovskite thin films deposited on glass and various SAM-modified FTO, and the resulting decay profiles were fitted using a biexponential decay function to extract average carrier lifetimes ( $\langle\tau\rangle$ ) using the formula,  $\langle\tau\rangle = \frac{A_1\tau_1^2 + A_2\tau_2^2}{A_1\tau_1 + A_2\tau_2}$ . Further, the decay rates were determined for the perovskite films deposited on glass and various SAM-modified FTO substrates using the formula,  $k_{\text{decay}} = 1/\langle\tau\rangle$ . Finally, the hole extraction rates for each SAM-modified FTO substrates were calculated using the formula:  $k_{\text{ext}} = k_{\text{decay, SAM}} - k_{\text{decay, perovskite}}$  assuming the additional decay is due to the hole transfer since the perovskite used is the same with only difference being the SAM modification of FTO.

### **(xiii) Contact Angle Measurements:**

The contact angle was measured using a contact angle meter (DCA-VZ, Kyowa Interface Science).

### **(xiii) Infrared (IR) Spectroscopy**

Infrared (IR) spectra of the SAMs deposited on FTO substrates were recorded using a Thermo Scientific Nicolet iS50 Fourier Transform Infrared (FTIR) spectrometer. The measurements were carried out in the range of 4000 – 400  $\text{cm}^{-1}$  to identify characteristic vibrational modes and confirm the adsorption of SAMs on the surface of FTO.

### **(xiv) Theoretical calculations**

Theoretical Calculations in order to optimize the molecular structure and to determine the dipole moment were performed using the Gaussian16 program.

#### **(xiv) Transient Photocurrent Decay (TPC) measurements**

Transient Photocurrent Decay (TPC) measurements were performed under short-circuit conditions using the all-in-one characterization platform Paios (Fluxim AG, Switzerland). A white light-emitting diode (LED) with a total optical power of 60 mW was used as the light source for these measurements.

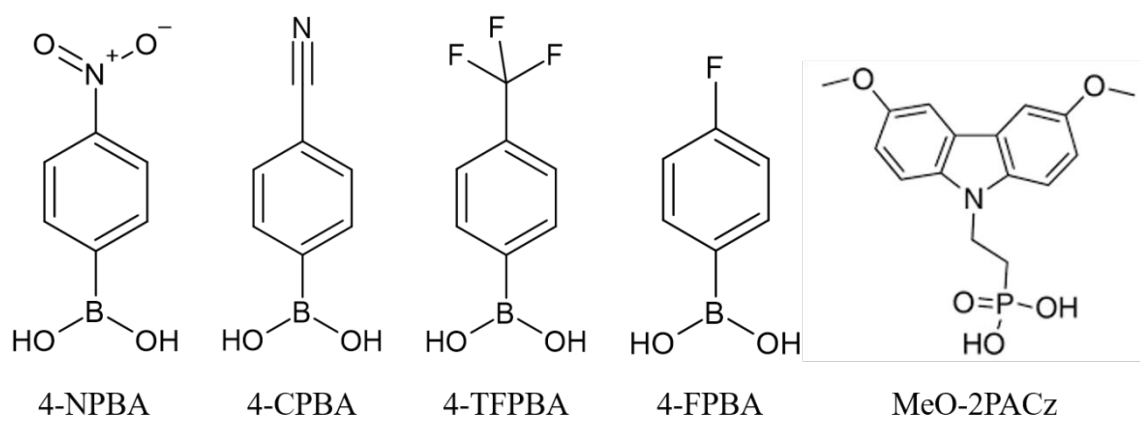


**Figure S1:** Molecular structures of Self-Assembled Monolayers (SAMs) used in this study.

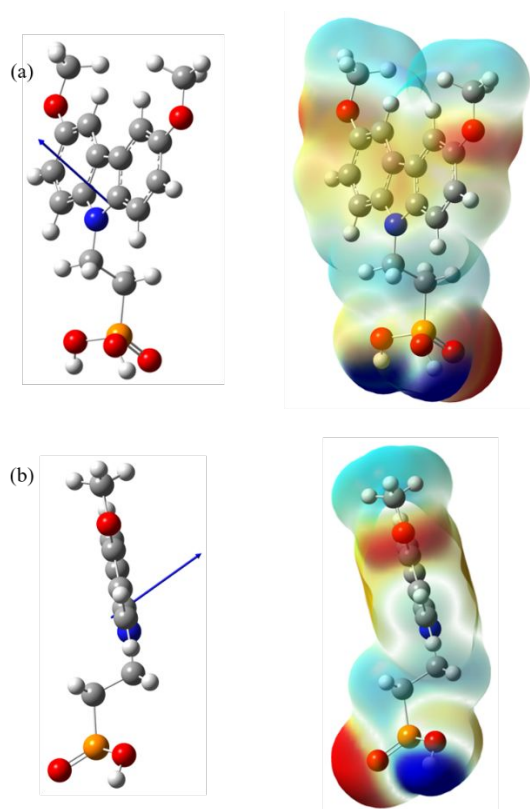


**Figure S2:** (a) Three quarter view and (b) Side view – of the Gaussian optimized molecular structure and Electrostatic Potential (ESP) map of MeO-2PACz.

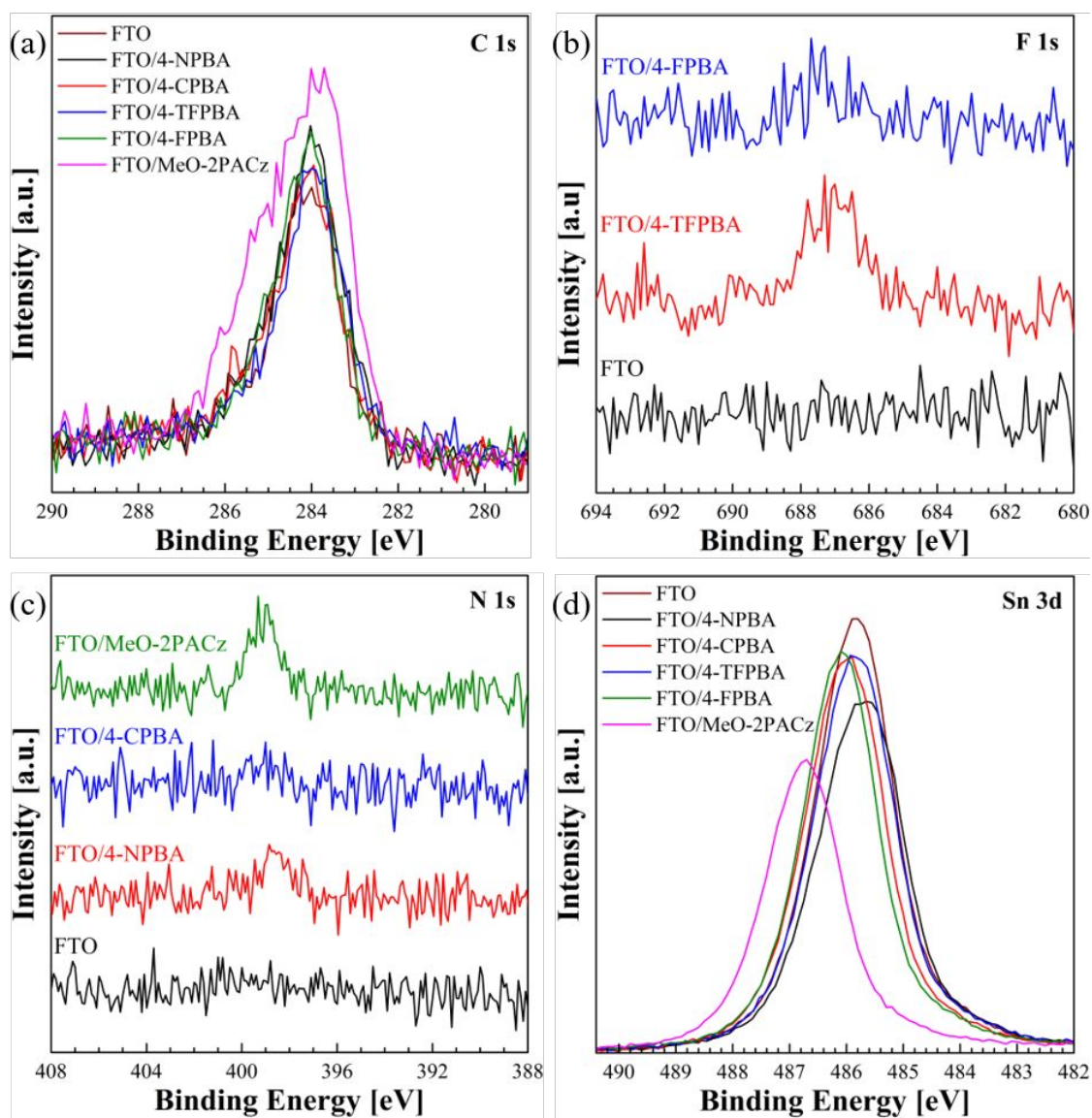


**Figure S3:** X-ray photoelectron spectra (XPS) showing (a) C 1s, (b) F 1s, (c) N 1s and (d) Sn 3d<sub>5/2</sub> peaks for bare FTO as well as for Self-Assembled Monolayers (SAMs) deposited on FTO.

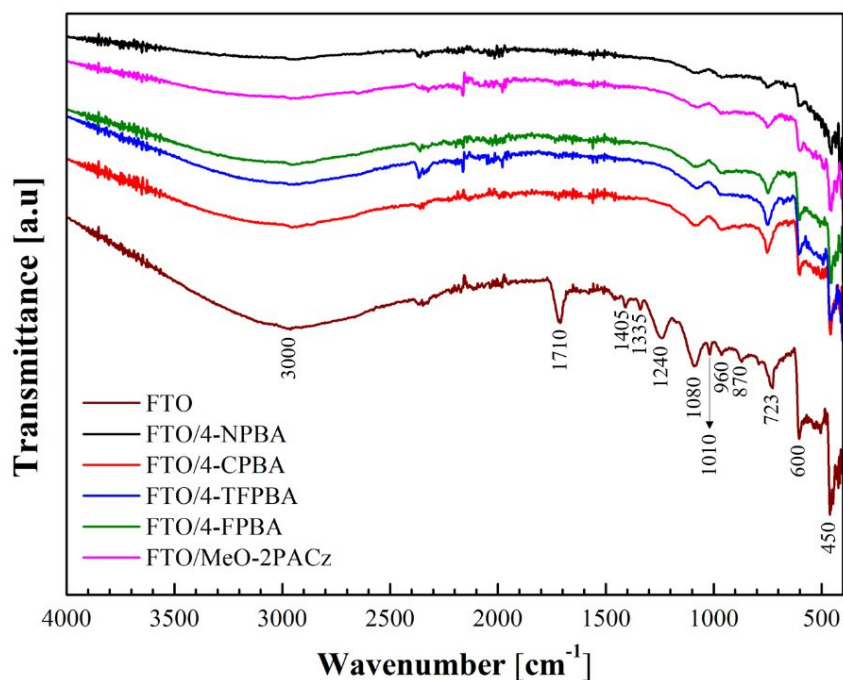


**Figure S4:** Infrared spectra of bare FTO and various SAM-modified FTO substrates confirming the existence of SAM on the surface of FTO.

Wavenumber (cm <sup>-1</sup> )	Assignment
450	Sn–O bending mode
600	Sn–O–Sn bridging or stretching
723	Surface Sn–O deformation
870	Sn–O–Sn asymmetric stretching
960	Sn–OH bending
1010	Sn–OH bending
1080	F–Sn–O or Sn–OH bending
1240	C–O asymmetric stretching
1335	CO <sub>3</sub> <sup>2-</sup> asymmetric stretching
1405	CO <sub>3</sub> <sup>2-</sup> asymmetric stretching or COO-symmetric stretching
1710	C=O stretching
3000	O–H stretching (broad)

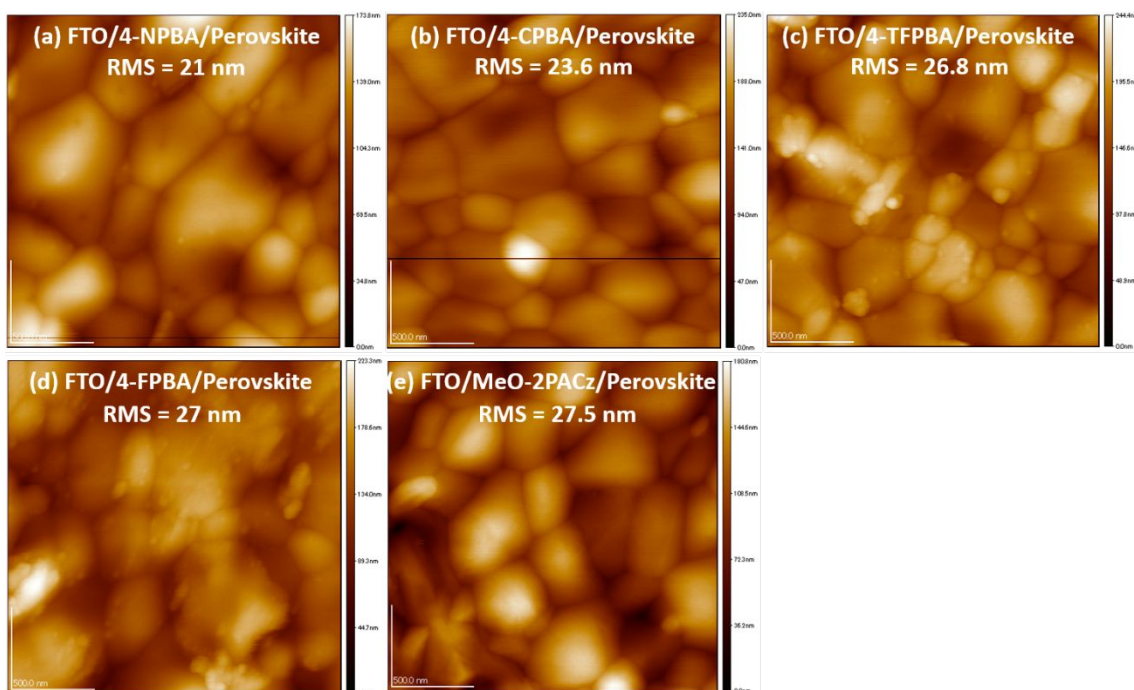


**Figure S5:** Atomic Force Microscopy (AFM) images showing surface roughness of perovskite films deposited on FTO substrates modified with (a) 4-NPBA, (b) 4-CPBA, (c) 4-TFPBA, (d) 4-FPBA and (e) MeO-2PACz.

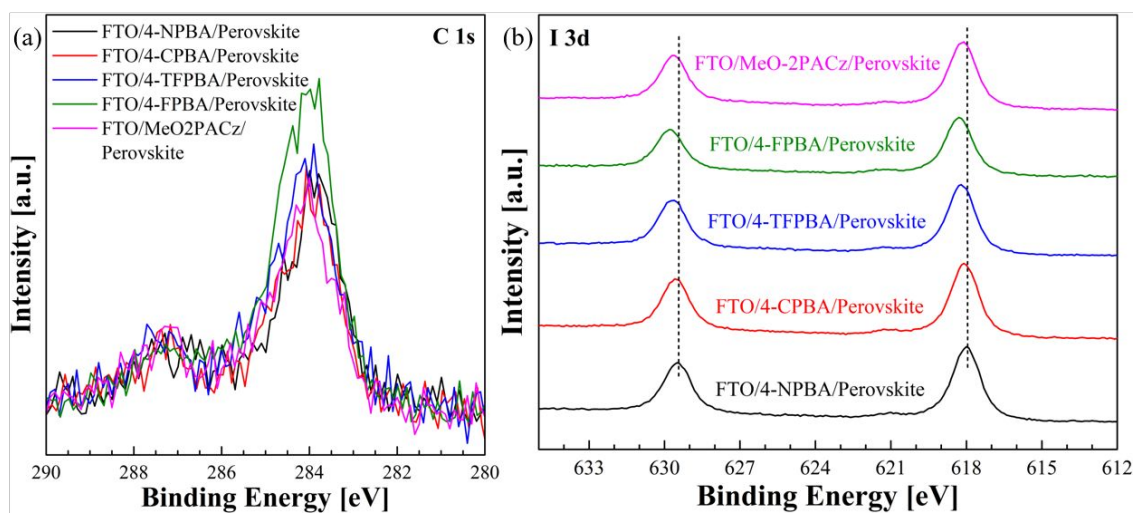


**Figure S6:** X-ray photoelectron spectra (XPS) showing (a) C 1s and (b) I 3d spectra of perovskite films deposited on various SAM-modified FTO substrates.

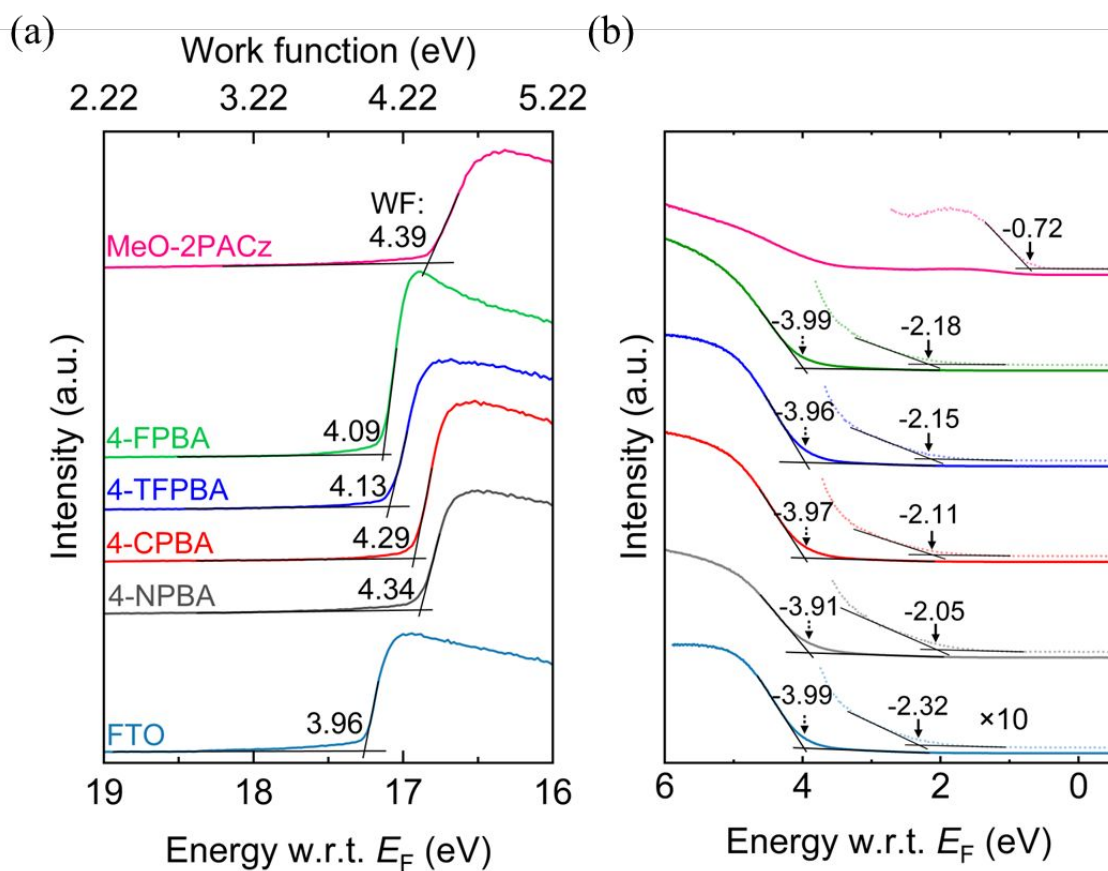
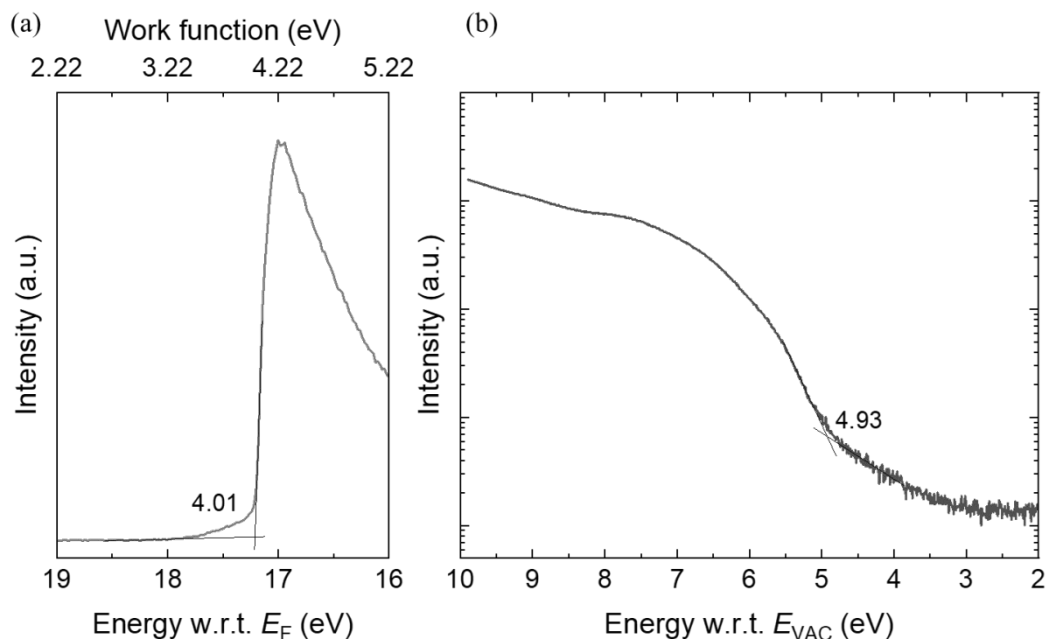


**Figure S7:** UPS spectra of (a) secondary electron cutoff (SECO) region, and (b) valence band maximum region for SAM-modified FTO substrates.

Figure S7a shows the secondary electron cutoff (SECO) region of UPS spectra for the bare and SAM-coated FTO substrates. The work functions (WF) derived from the SECO were 3.96 eV for FTO, 4.39 eV for MeO-2PACz, 4.34 eV for 4-NPBA, 4.29 eV for 4-CPBA, 4.13 eV for 4-TFPBA, and 4.09 eV for 4-FPBA. Among these SAMs, MeO-2PACz on FTO showed the largest WF. The order of WFs among the BA-based SAMs corresponded to the order of WFs corresponded to that of the dipole moments of the isolated molecules, as calculated by DFT (Figure 1a).

Figure S7b shows the valence band region spectra with the energy with respect to Fermi level. For MeO-2PACz, a clear onset corresponding to the HOMO level was observed at  $-0.72$  eV. In contrast, two possible onset positions were identified for BA-based SAMs, an intense onset around  $-4$  eV, indicated by the dotted arrow, and a weak onset around  $-2$  eV, indicated by the solid arrow. The onset positions indicated by the dotted arrows were  $-3.99$  eV for the FTO substrate,  $-3.91$  eV for 4-NPBA,  $-3.97$  eV for 4-CPBA,  $-3.96$  eV for 4-TFPBA, and  $-3.99$  eV for 4-FPBA. These features closely resemble both the spectral shape and onset position of the FTO substrate, and likely originate from the signal from the FTO substrate rather than the HOMO level of the BA-based SAMs. In fact, the onset feature at  $-4$  eV is less clear in MeO-2PACz, meaning that the molecular adsorption density is lower in the BA-based SAM than that in MeO-2PACz. This low coverage of the BA-based SAM is supported by N1s core levels observed by XPS as shown in Figure S13, indicating that the adsorption density of the BA-based SAM is approximately one-quarter that of the MeO-2PACz.

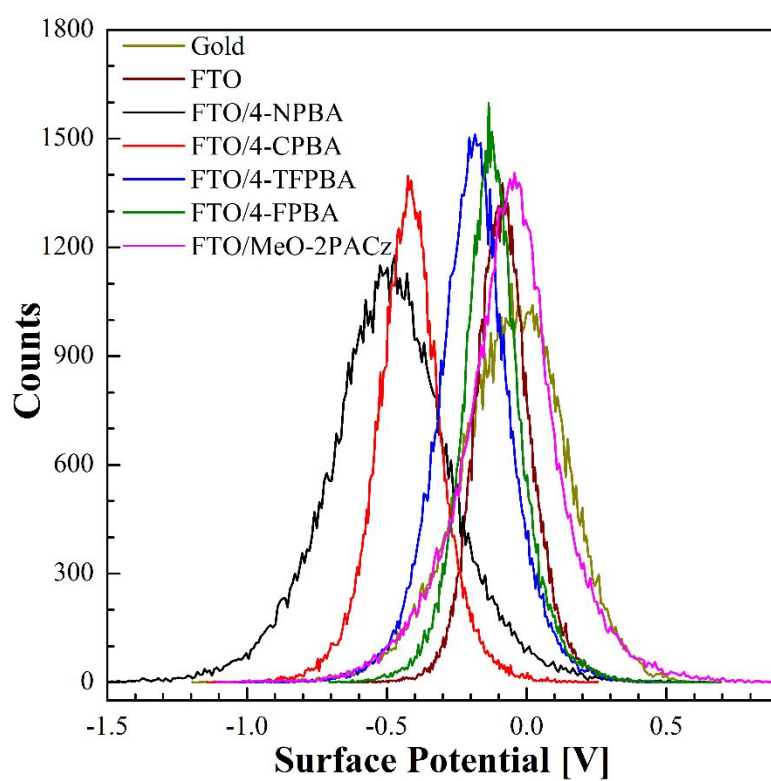
The onset positions indicated by the solid arrows were  $-2.32$  eV for the FTO substrate,  $-2.05$  eV for 4-NPBA,  $-2.11$  eV for 4-CPBA,  $-2.15$  eV for 4-TFPBA, and  $-2.18$  eV for 4-FPBA. As the sum of these values and the respective work functions, we calculated the ionization energies (IE) as  $6.28$  eV for the FTO substrate,  $6.39$  eV for 4-NPBA,  $6.40$  eV for 4-CPBA,  $6.28$  eV for 4-TFPBA, and  $6.27$  eV for 4-FPBA. These values were in good agreement with the results obtained from photoelectron yield spectroscopy (PYS) measurements shown in Figure S10. The good agreement between the UPS and PYS measurements further support the assignment of these spectral features around  $-2$  eV in UPS as the valence band maximum (VBM).



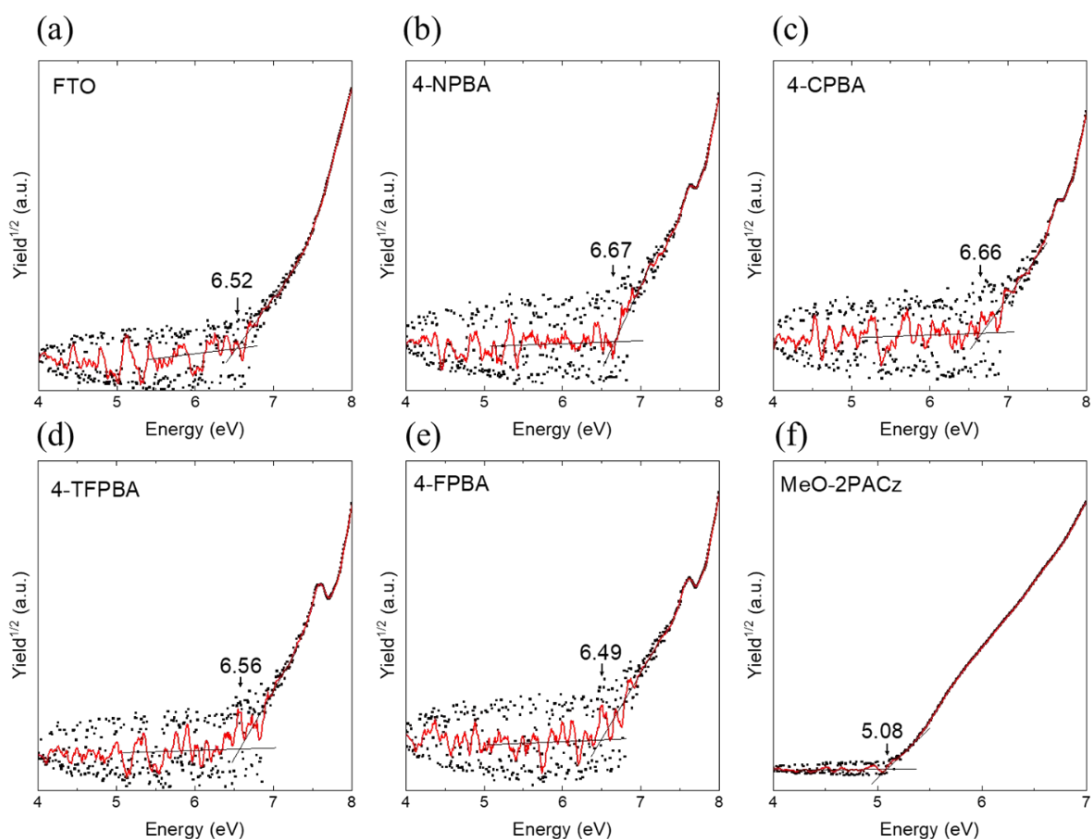
**Figure S8:** UPS spectra of (a) secondary electron cutoff (SECO) region, and (b) Valence band maximum region for Sn-Pb perovskite ( $\text{Cs}_{0.15}\text{FA}_{0.8}\text{Rb}_{0.05}\text{Sn}_{0.25}\text{Pb}_{0.75}\text{I}_{2.5}\text{Br}_{0.5}$ ) deposited on bare FTO. (a) and (b) are plotted with linear and semi-log scale, respectively.

Figure S8 shows UPS spectrum of the Sn-Pb perovskite ( $\text{Cs}_{0.15}\text{FA}_{0.8}\text{Rb}_{0.05}\text{Sn}_{0.25}\text{Pb}_{0.75}\text{I}_{2.5}\text{Br}_{0.5}$ ). From the panels (a) and (b), we determined the WF and VBM, respectively. The WF was 4.01 eV. To determine VB, we plotted the UPS spectrum on a logarithmic scale, as proposed previously<sup>1,2</sup>. The determined ionization energy of  $\text{Cs}_{0.15}\text{FA}_{0.8}\text{Rb}_{0.05}\text{Sn}_{0.25}\text{Pb}_{0.75}\text{I}_{2.5}\text{Br}_{0.5}$  is 4.93 eV.

[Note: Although exposure of the samples to ambient air was minimized as much as possible, we acknowledge that Sn-Pb perovskite surfaces are prone to oxidation, which may influence the accuracy of surface electronic measurements.]



**Figure S9:** (a) Surface potential plot for Gold (reference), bare FTO and various SAM-modified FTO acquired obtain from KPFM measurements.



**Figure S10:** Photoelectron Yield Spectra (PYS) for (a) bare FTO and (b) 4-NPBA, (c) 4-CPBA, (d) 4-TFPBA, (e) 4-FPBA and (f) MeO-2PACz – modified FTO substrate.

Figure S10 presents the PYS measurement results. The ionization energies for each sample were determined to be 6.52 eV for the FTO substrate, 6.67 eV for 4-NPBA, 6.66 eV for 4-CPBA, 6.56 eV for 4-TFPBA, 6.49 eV for 4-FPBA, and 5.08 eV for MeO-2PACz. For all spectra, a single 15-point smoothing procedure was applied prior to determining the onset positions.

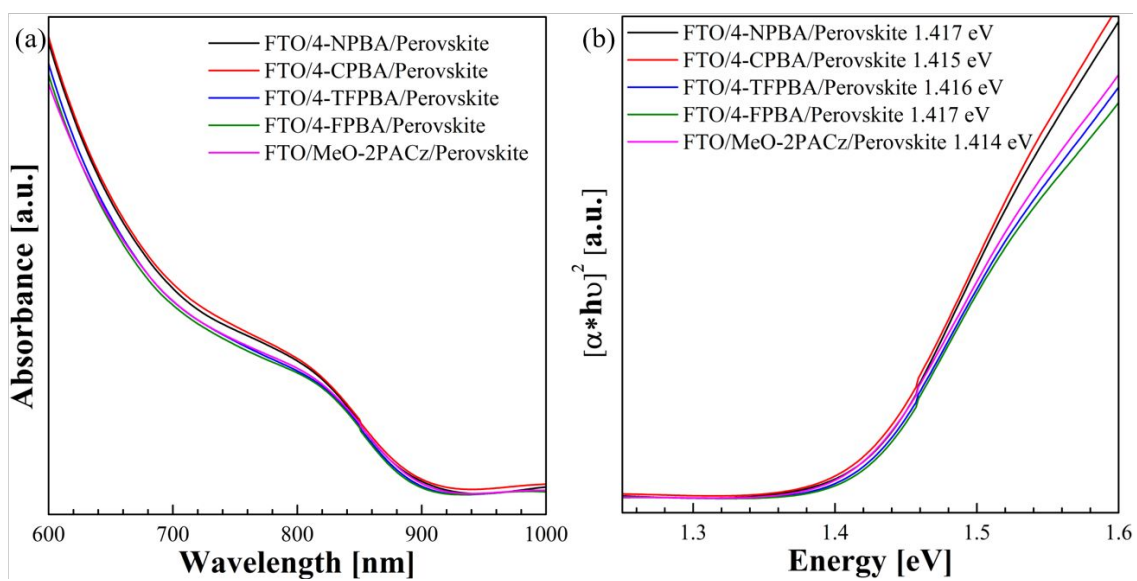


**Figure S11:** (a) UV-visible absorption spectra of perovskite films deposited on various SAM-modified FTO substrates; (b) Tauc plot of perovskite films deposited on various SAM-modified FTO substrates.

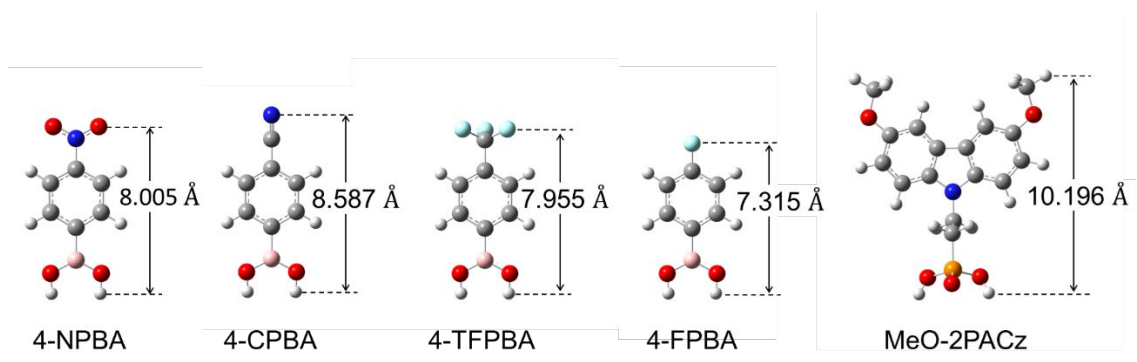


**Figure S12:** Lengths of BA-based SAMs and MeO-2PACz calculated by the DFT method.

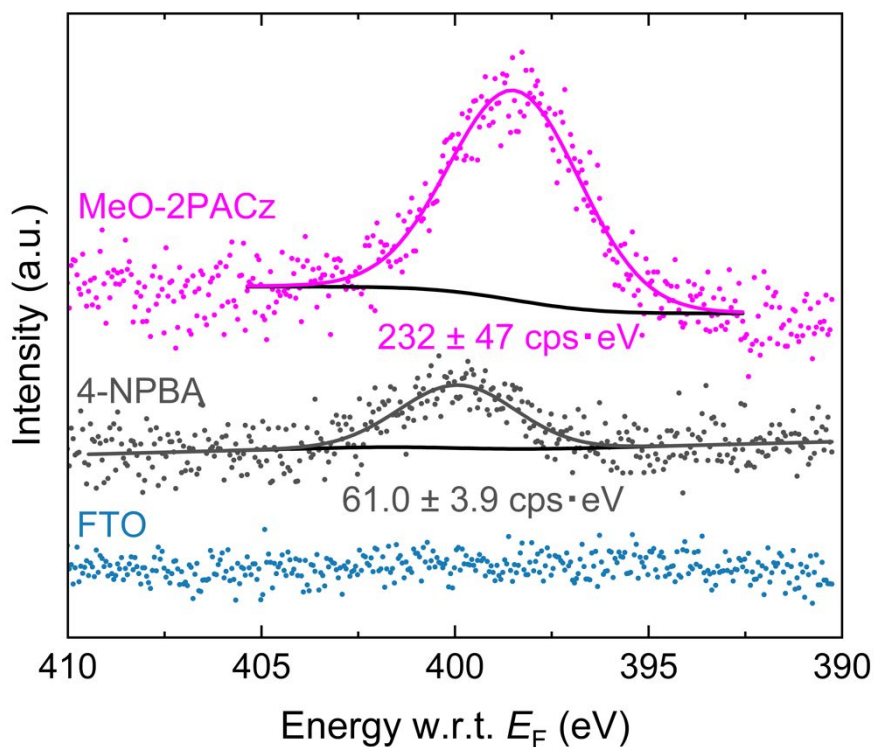


**Figure S13:** XPS spectra of the N 1s region for 4-NPBA and MeO-2PACz.

Figure S13 shows the XPS spectra of the N 1s core-level for 4-NPBA and MeO-2PACz. The baseline was subtracted using the Shirley method. The N 1s peak areas for 4-NPBA and MeO-2PACz were  $61.0 \pm 3.9$  and  $232 \pm 47$ , respectively. Since both molecules contain one nitrogen atom per molecule, the adsorption density of 4-NPBA is estimated to be approximately one-fourth that of MeO-2PACz.

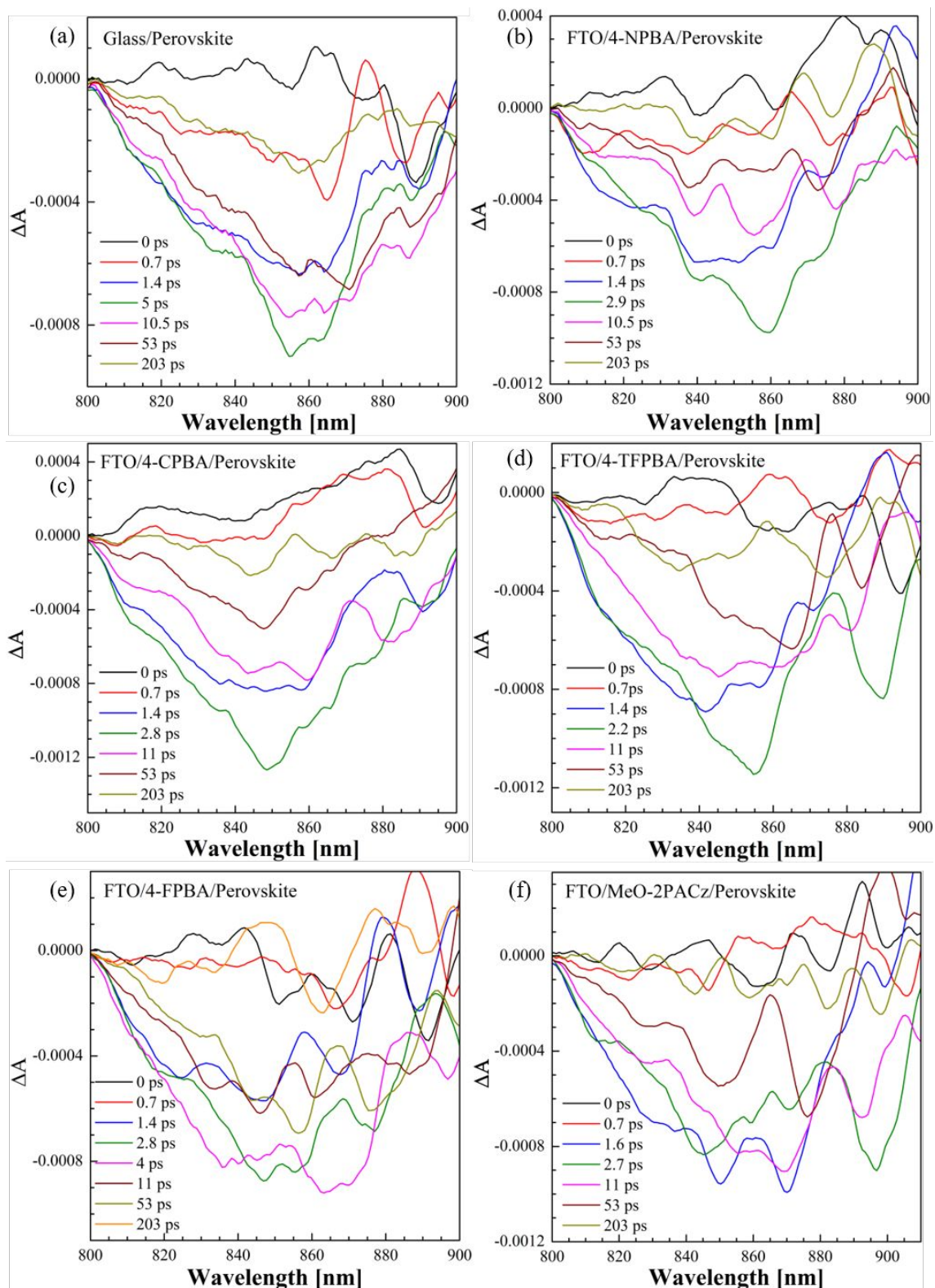


**Figure S14:** Transient Absorption spectra of perovskite deposited on (a) glass, and (b) 4-NPBA, (c) 4-CPBA, (d) 4-TFPBA, (e) 4-FPBA and (f) MeO-2PACz – modified FTO.

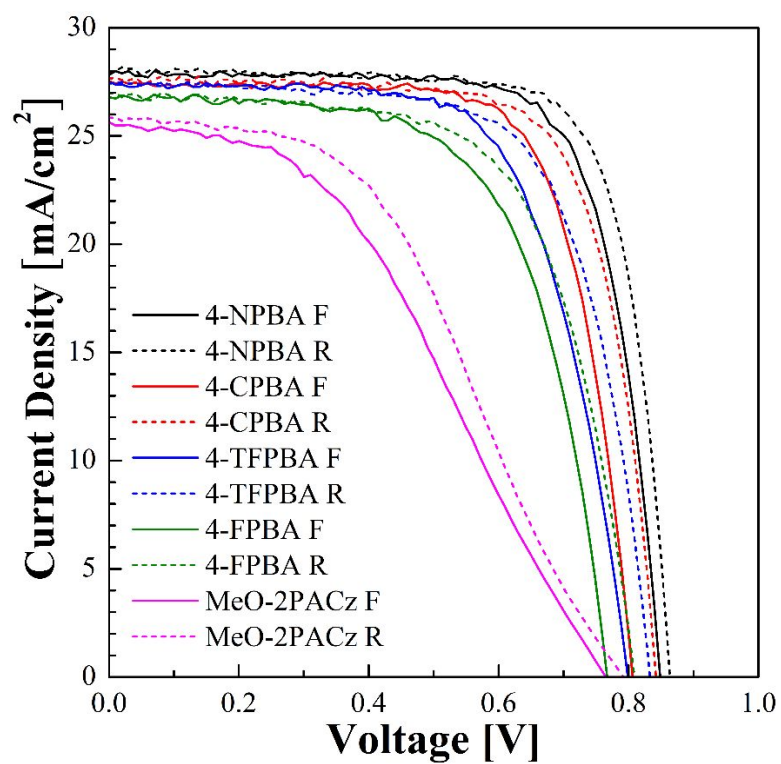


**Figure S15:** Current-Voltage (I-V) spectra under both forward and reverse scan for the PSCs fabricated on various SAM-modified FTO substrates.

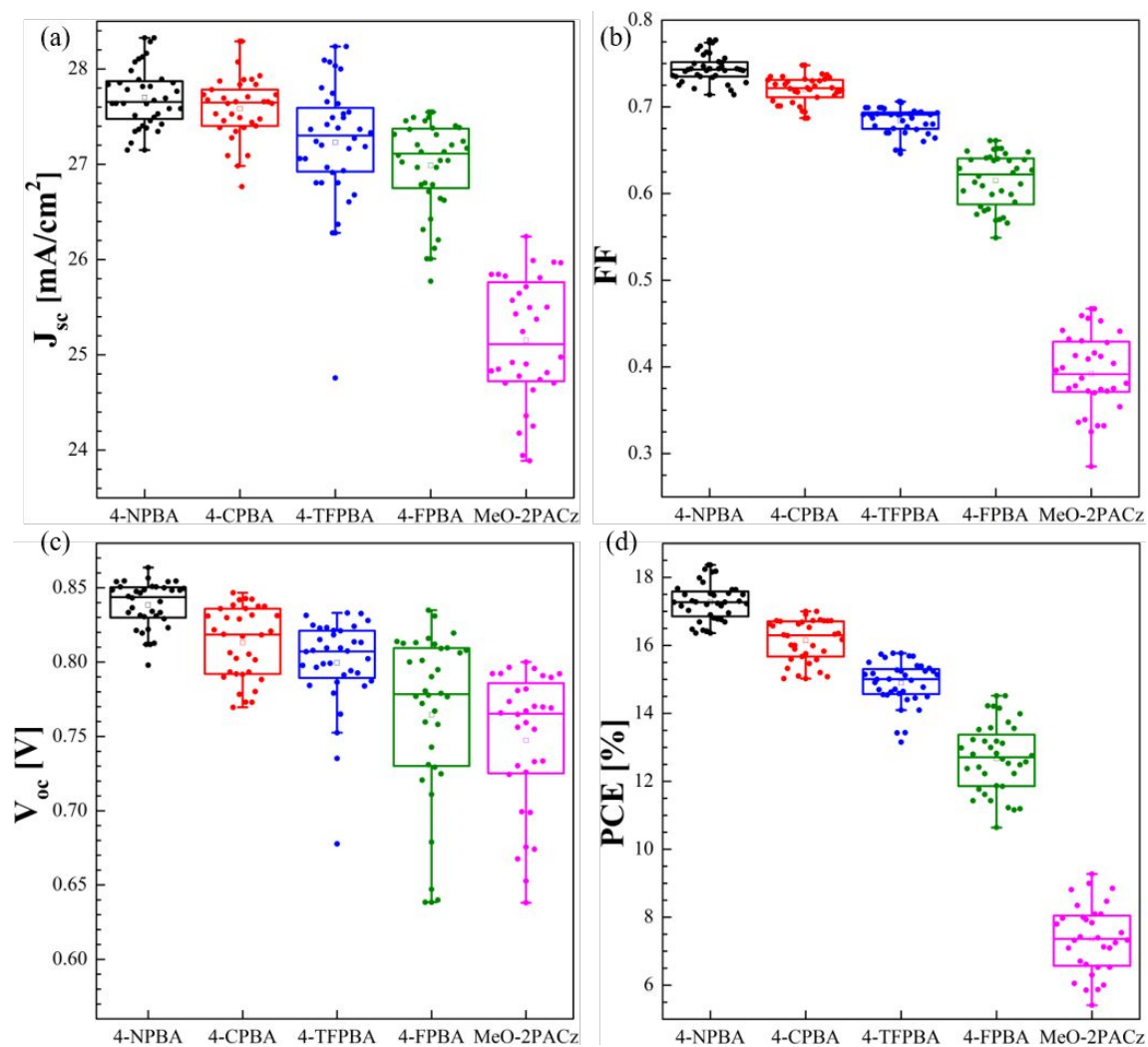


**Figure S16:** Box chart showing (a) power conversion efficiency (PCE), (b) fill-factor (FF), (c) open-circuit voltage ( $V_{oc}$ ), and (d) short-circuit current density ( $J_{sc}$ ) of 18 independent PSCs.

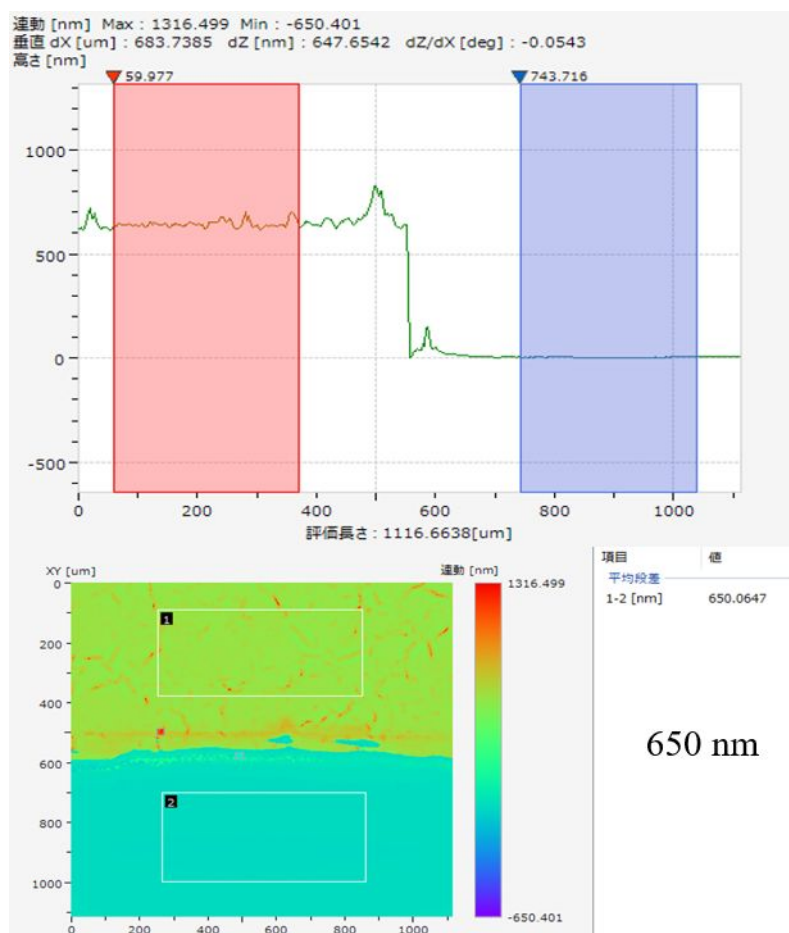


**Figure S17:** Thickness of the perovskite film used in this study. (The perovskite film was deposited on bare glass substrate for precise thickness measurement)

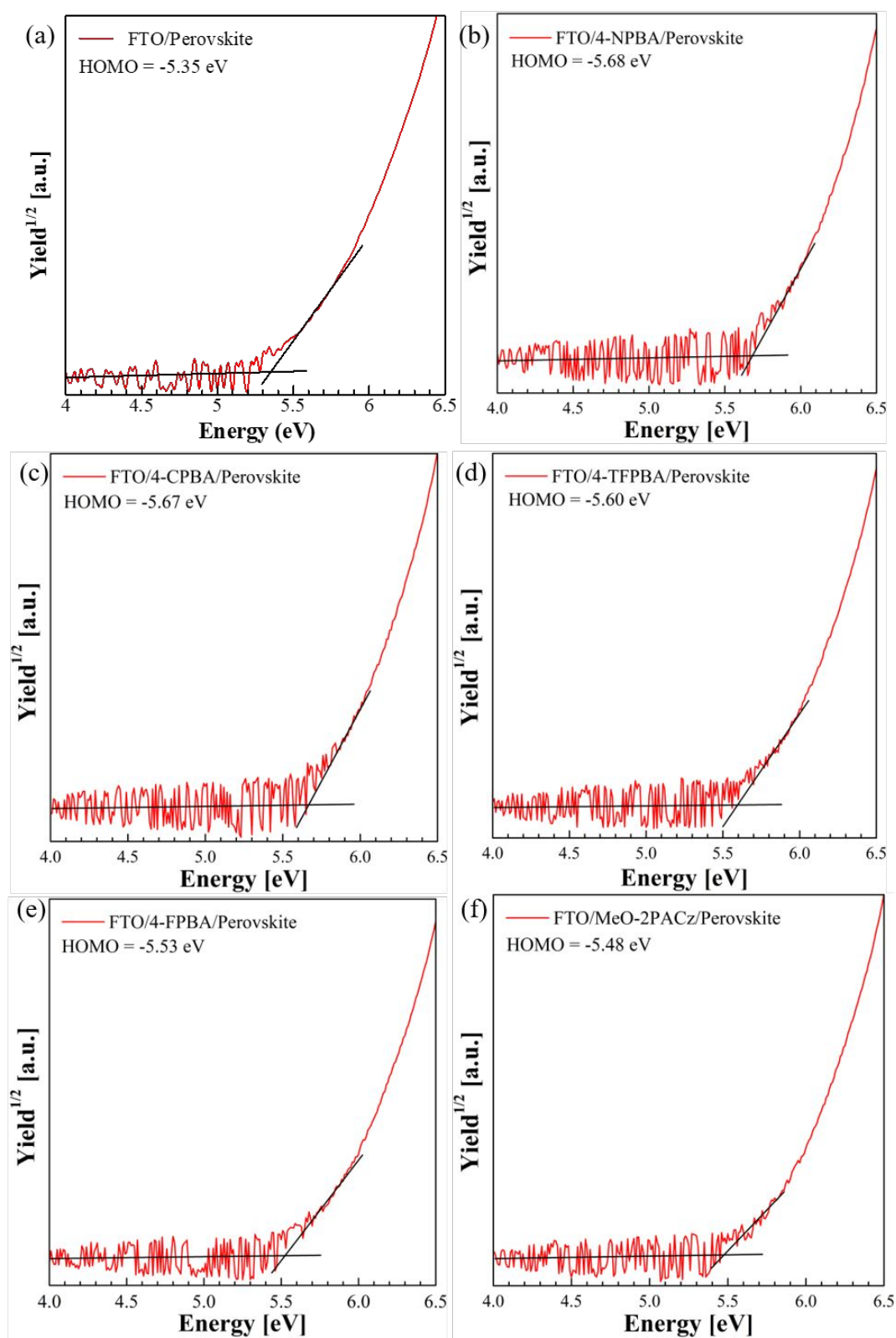


**Figure S18:** PYS spectra of perovskite film deposited on (a) bare FTO, (b) 4-NPBA, (c) 4-CPBA, (d) 4-TFPBA, (e) 4-FPBA and (f) MeO-2PACz-modified FTO.

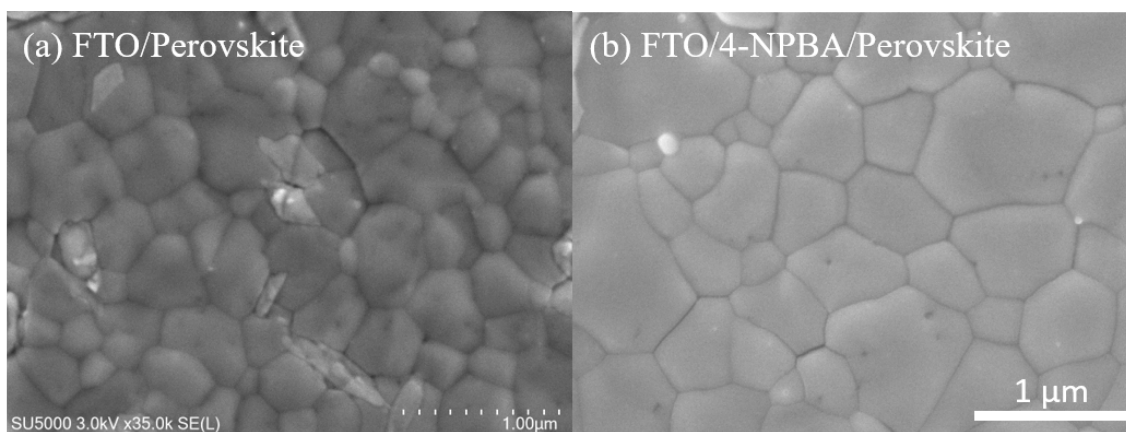


**Figure S19:** Comparison of surface morphology of perovskite films deposited on bare FTO substrate with those deposited on 4-NPBA-modified FTO substrate.

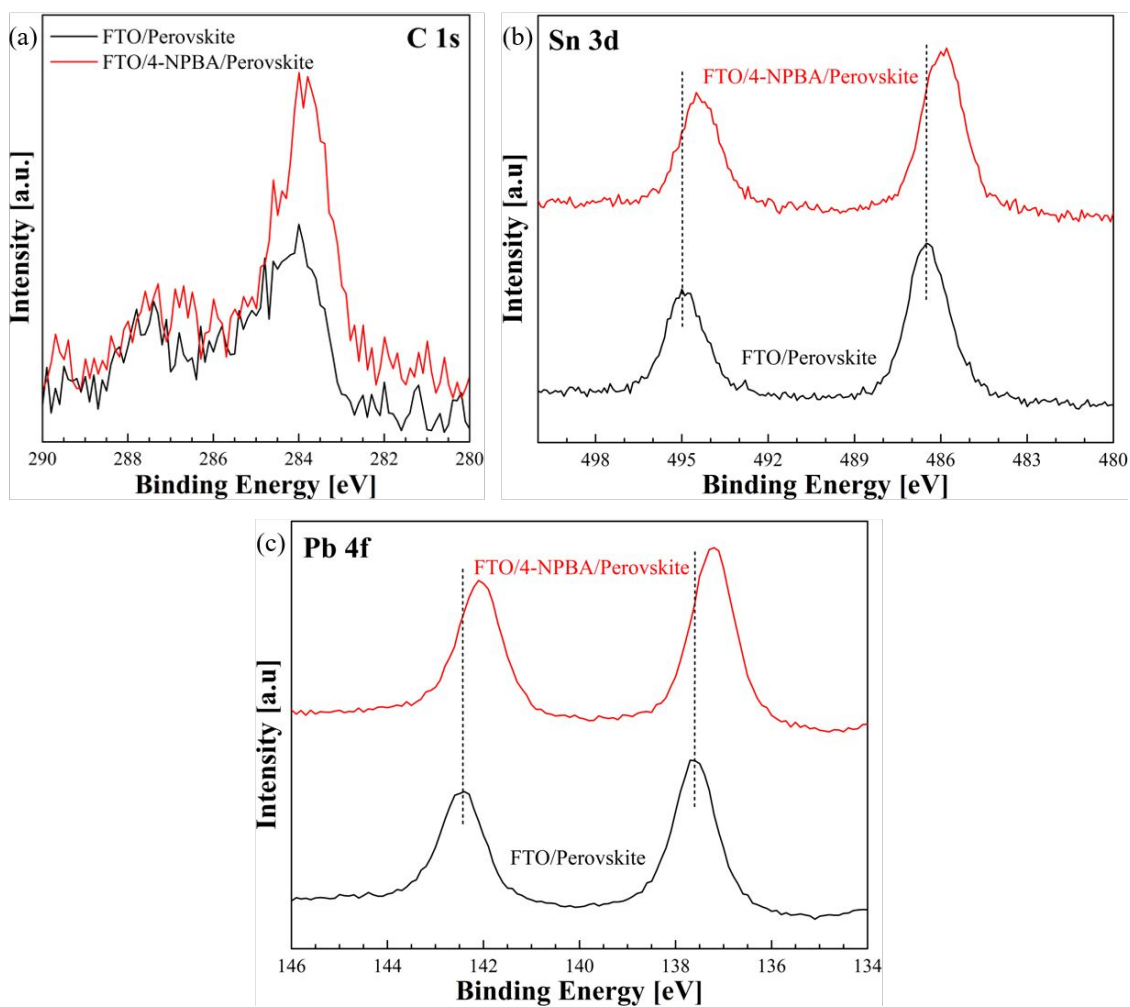


**Figure S20:** Comparison of (a) C 1s, (b) Sn 3d, (c) Pb 4f spectra for perovskite films deposited on bare FTO substrate with those deposited on 4-NPBA-modified FTO substrate.

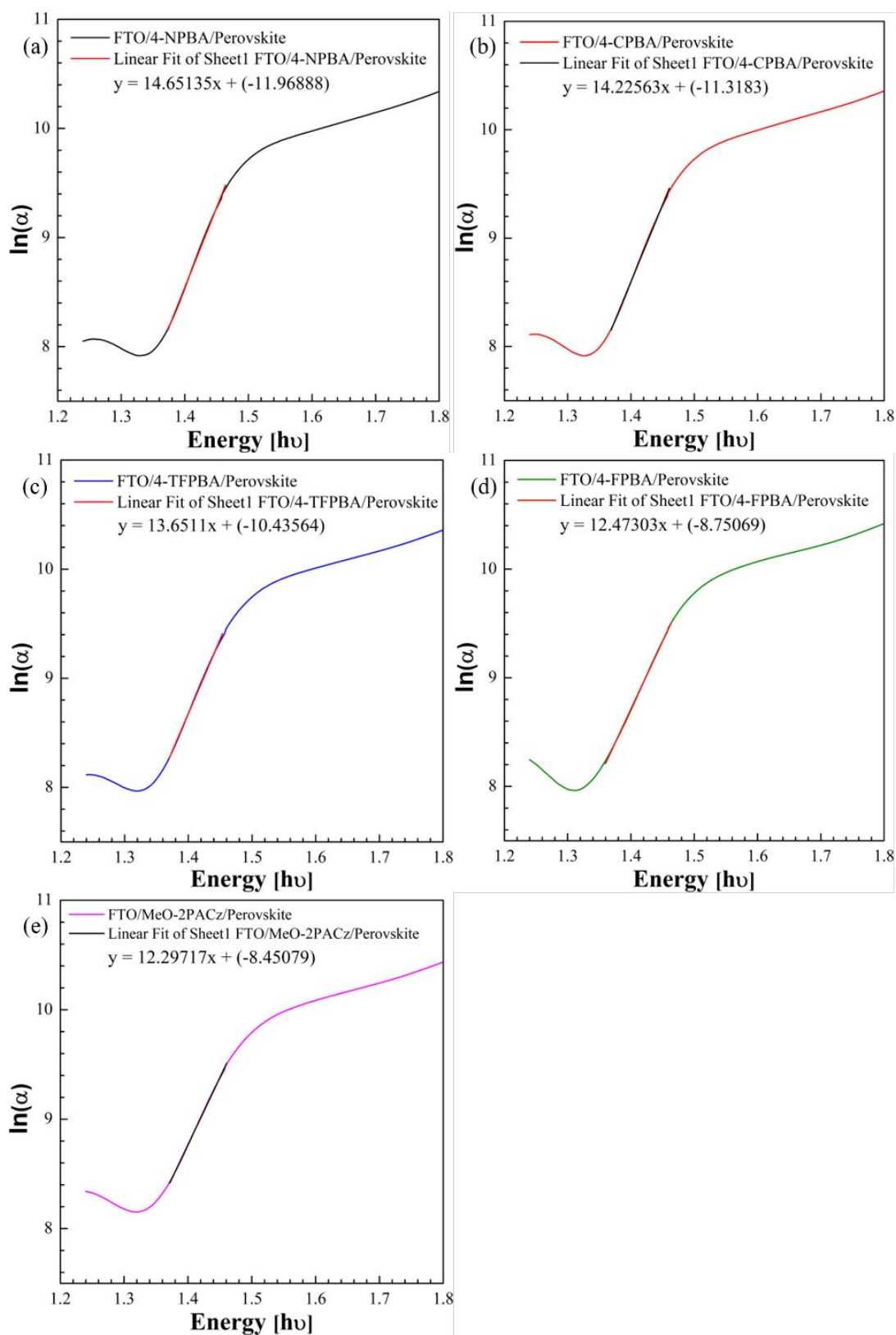


**Figure S21:** Urbach Energy Analysis for the perovskite film deposited on FTO substrate modified by (a) 4-NPBA, (b) 4-CPBA, (c) 4-TFPBA, (d) 4-FPBA and (e) MeO-2PACz.

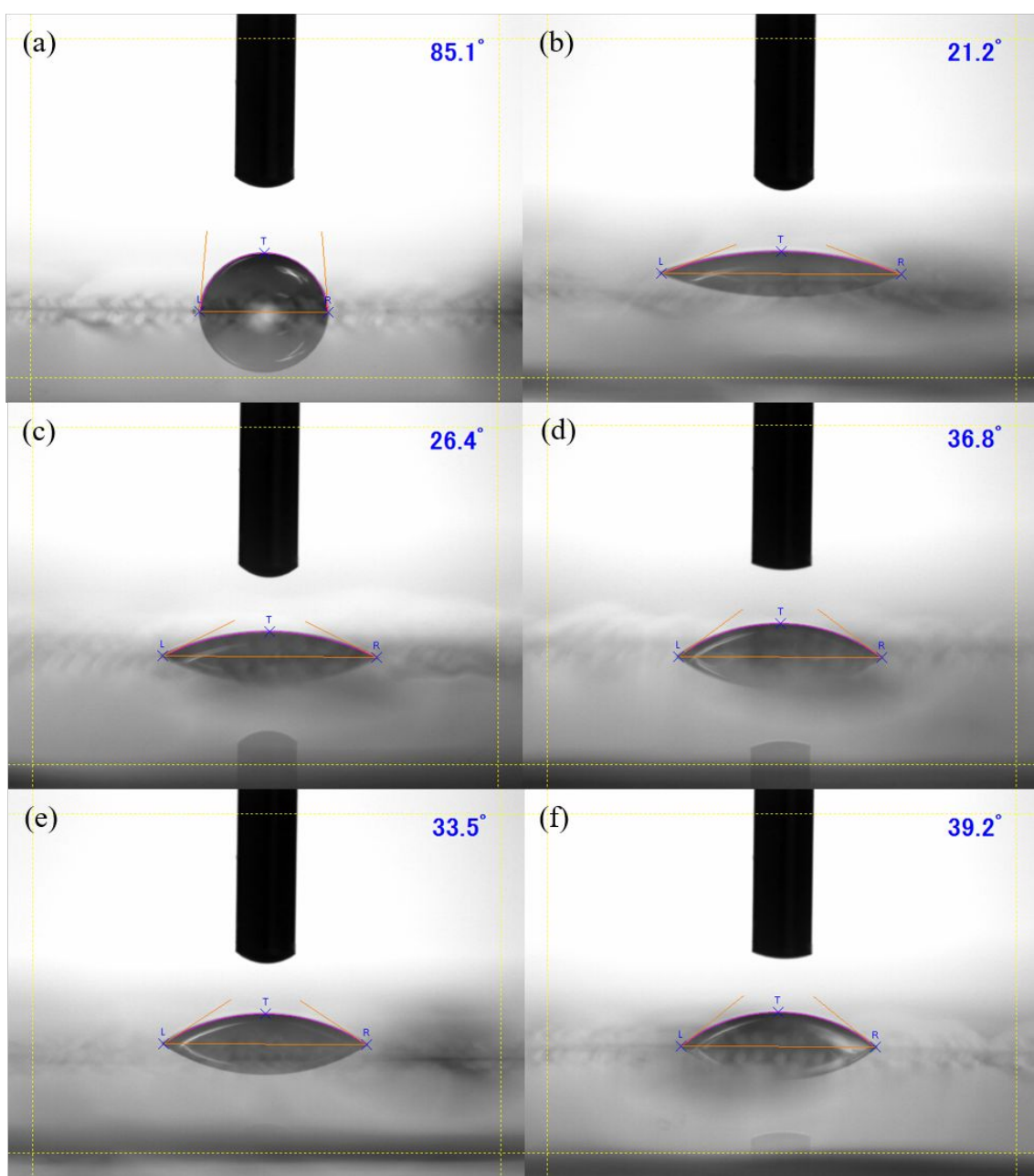


**Figure S22:** Contact Angle of water on (a) bare FTO and FTO substrates modified with (b) 4-NPBA, (c) 4-CPBA, (d) 4-TFPBA, (e) 4-FPBA and (f) MeO-2PACz.

**Table S1:** Structural parameters for the (100) diffraction peak of perovskite films deposited on FTO substrates modified with different SAMs, obtained from XRD peak fitting.

	2 $\theta$ (°)	(hkl)	d-spacing (Å)	FWHM (°)	Crystal size (Å)
FTO/4-NPBA/Perovskite	14.584	(100)	6.0689	0.0975	858.17
FTO/4-CPBA/Perovskite	14.586	(100)	6.0681	0.1231	679.41
FTO/4-TFPBA/Perovskite	14.585	(100)	6.0684	0.1192	701.98
FTO/4-FPBA/Perovskite	14.587	(100)	6.0676	0.1138	734.80
FTO/MeO-2PACz/Perovskite	14.580	(100)	6.0704	0.1201	697.57

**Table S2:** Determination of work function of various SAM layers deposited on FTO substrate determined using Kelvin Probe Force Microscopy method.

	Surface potential (V)	Counts	$\Delta V_{\text{SAM}}$ (V)	$\Delta \Phi_{\text{SAM}}$ (eV)	$\Phi_{\text{SAM}}$ (eV)	$E_{\text{F(SAM)}}$ (eV)
Gold	-0.05317	1100	-	-	-	-
Bare FTO	-0.8616	1405	-0.03299	0.03299	5.13299	-5.13299
4-NPBA	-0.47102	1178	-0.41785	0.41785	5.51785	-5.51785
4-CPBA	-0.42425	1397	-0.37108	0.37108	5.47108	-5.47108
4-TFPBA	-0.18451	1511	-0.13134	0.13134	5.23134	-5.23134
4-FPBA	-0.13527	1598	-0.0821	0.0821	5.1821	-5.1821
MeO-2PACz	-0.043	1405	0.01017	-0.01017	5.08983	-5.08983

$$\Delta V_{\text{SAM}} = V_{\text{SAM}} - V_{\text{Au}}$$

$$\Delta \Phi_{\text{SAM}} = -e * \Delta V_{\text{SAM}} [e = 1.0 \text{ eV/V}]$$

$$\Phi_{\text{SAM}} = \Phi_{\text{Au}} + \Delta \Phi_{\text{SAM}} [\Phi_{\text{Au}} = 5.1 \text{ eV}]$$

$$E_{\text{F(SAM)}} = -\Phi_{\text{SAM}}$$

**Table S3:** Estimated tunnelling probabilities for BA-based SAMs at different titling angles.

Transmittance calculated results				
Normal	1.87 %	1.40 %	2.32 %	6.94 %
30° w.r.t. Normal	3.64 %	2.83 %	4.36 %	9.86 %
45° w.r.t. Normal	6.47 %	5.20 %	7.50 %	13.6 %
60° w.r.t. Normal	10.6 %	8.75 %	11.9 %	18.1 %

**Table S4:** Average carrier lifetime, decay rates and hole extraction rates calculated by fitting the kinetic trace extracted from Ground State Bleach (GSB) in the Transient Absorption (TA) spectra of perovskite films deposited on glass as well as various SAM-modified FTO.

	$A_1$	$\tau_1$	$A_2$	$\tau_2$	$\langle\tau\rangle$ (ps)	$k_{\text{decay}}$ ( $\times 10^{-3}$ ps)	$k_{\text{ext}}$ ( $\times 10^{-3}$ ps)
Glass/PVK	0.511	121.662	0.308	1100.904	949.144	1.054	
FTO/4-NPBA/Perovskite	0.584	33.501	0.296	254.774	209.256	4.779	3.725
FTO/4-CPBA/Perovskite	0.447	42.336	0.347	340.073	298.934	3.345	2.292
FTO/4-TFPBA/Perovskite	0.433	65.975	0.372	417.593	362.864	2.756	1.702
FTO/4-FPBA/Perovskite	0.508	44.506	0.309	433.638	377.526	2.649	1.595
FTO/MeO2-PACz/Perovskite	0.510	57.685	0.332	568.68	499.778	2.001	0.947

Model: ExpDec2

$$\text{Equation: } y = A_1 e^{-x/\tau_1} + A_2 e^{-x/\tau_2} + y_0$$

$$\langle\tau\rangle = \frac{A_1 \tau_1^2 + A_2 \tau_2^2}{A_1 \tau_1 + A_2 \tau_2}$$

$$k_{\text{decay}} = 1/\langle\tau\rangle$$

$$k_{\text{ext}} = k_{\text{decay, SAM}} - k_{\text{decay, perovskite}}$$

**Table S5:** Charge transport time ( $t_{\text{TPC,tr}}$ ) determined by fitting the transient photocurrent (TPC) decay curves of perovskite solar cells (PSCs) fabricated on various SAM-modified FTO substrates. All other device components including the FTO, perovskite absorber, electron transport layers (PCBM, C<sub>60</sub>, and BCP), and silver (Ag) electrode were kept identical, with only the SAM layer varied to isolate its influence on charge transport.

	Adj. R-Square	A <sub>1</sub>	$\tau_1$
FTO/4-NPBA	0.99444	1.14564	1.184
FTO/4-CPBA	0.99309	1.13057	2.008
FTO/4-TFPBA	0.99246	1.10189	3.846
FTO/4-FPBA	0.99683	1.04461	4.714
FTO/MeO2-PACz	0.99009	1.13456	10.583

Model: ExpDec1

$$\text{Equation: } y = A_1 e^{-x/\tau_1} + y_0$$

**Table S6:** Photovoltaic parameters of PSCs fabricated on different SAM-modified FTO substrates.

SAM		$J_{sc}$ [mA/cm <sup>2</sup> ]	Integrated $J_{sc}$ [mA/cm <sup>2</sup> ]	$V_{oc}$ [V]	FF	PCE [%]
4-NPBA	Forward	27.816	27.290	0.8486	0.742	17.526
	Reverse	27.888		0.8636	0.763	18.367
4-CPBA	Forward	27.529	27.216	0.8063	0.721	16.002
	Reverse	27.656		0.8423	0.73	16.999
4-TFPBA	Forward	27.489	27.099	0.7989	0.67	14.708
	Reverse	27.417		0.8331	0.687	15.688
4-FPBA	Forward	26.786	26.543	0.7671	0.642	13.182
	Reverse	26.968		0.8092	0.651	14.209
MeO-PACz	Forward	25.646	25.755	0.7649	0.412	8.091
	Reverse	25.845		0.7922	0.453	9.269

**Table S7:** Tabulated values of Urbach Energy ( $E_u$ ) for the perovskite films coated on FTO substrate modified by (a) 4-NPBA, (b) 4-CPBA, (c) 4-TFPBA, (d) 4-FPBA and (e) MeO-2PACz.

	Slope	Urbach Energy (eV)	Urbach Energy (meV)
FTO/4-NPBA/Perovskite	14.65135	0.068253	68.2531
FTO/4-CPBA/Perovskite	14.22563	0.070296	70.29566
FTO/4-TFPBA/Perovskite	13.6511	0.073254	73.25417
FTO/4-FPBA/Perovskite	12.47303	0.080173	80.17298
FTO/MeO-2PACz/Perovskite	12.29717	0.08132	81.31952

## References

- (1) Endres, J.; Egger, D. A.; Kulbak, M.; Kerner, R. A.; Zhao, L.; Silver, S. H.; Hodes, G.; Rand, B. P.; Cahen, D.; Kronik, L.; Kahn, A. Valence and Conduction Band Densities of States of Metal Halide Perovskites: A Combined Experimental–Theoretical Study. *J. Phys. Chem. Lett.* **2016**, *7* (14), 2722–2729. <https://doi.org/10.1021/acs.jpcclett.6b00946>.
- (2) Zu, F.; Amsalem, P.; Egger, D. A.; Wang, R.; Wolff, C. M.; Fang, H.; Loi, M. A.; Neher, D.; Kronik, L.; Duhm, S.; Koch, N. Constructing the Electronic Structure of CH<sub>3</sub>NH<sub>3</sub>PbI<sub>3</sub> and CH<sub>3</sub>NH<sub>3</sub>PbBr<sub>3</sub> Perovskite Thin Films from Single-Crystal Band Structure Measurements. *J. Phys. Chem. Lett.* **2019**, *10* (3), 601–609. <https://doi.org/10.1021/acs.jpcclett.8b03728>.